Modeling and Equilibrium Studies for the Adsorption of Congo red Using *Detarium microcarpum* Seed Shell Activated Carbon

Musa Husaini, Bishir Usman and Muhammad Bashir Ibrahim

Department of Pure and Industrial Chemistry, Faculty of Physical Sciences College of Natural and Pharmaceutical Sciences, Bayero University Kano (BUK), P.M.B. 3011, Kano, Nigeria.

Corresponding author. E-mail address: mbibrahim.chm@buk.edu.ng

Abstarct

Activated carbon obtained from *Detarium microcarpum* seed shell (SDAC) was used to eliminate Congo red (CR) from an aqueous solution using batch adsorption method. Various characterization techniques, including SEM, FT-IR and pH at point of zero charge (pH_{pzc}) were employed to characterize the adsorbent surface. The study investigated several adsorption parameters, namely contact time (5 - 150 minutes), temperature (303 - 323 K), and initial concentration (20 - 500 mg/L). The adsorption data were analyzed using kinetic, isotherm, and thermodynamic equations. The kinetics of the process conformed well to the pseudo-second-order model, indicating that both external and internal diffusion influenced the adsorption of the dye onto the adsorbent. The isotherm data aligned with the Freundlich model, suggesting that CR formed multiple layers on the heterogeneous surface of the adsorbent. The values of thermodynamic calculations ΔS = -0.139 kJ/mol, ΔH = - 48.77 kJ/K demonstrates the feasibility and exothermic nature of the dye adsorption process and the values of ΔG = -6.52, -5.82, -5.12, -4.42 and -3.73 kJ/mol obtained at various temperature confirmed the spontaneity of the entire adsorption process.

1. Introduction

Water contamination with various pollutants, including toxic heavy metals and dyes, poses significant risks to human health [1]. One major class of synthetic colorants, azo dyes like congo red, is extensively used in textile manufacturing due to their wide range of shades, resistance to fading, and low energy consumption [2]. Azo dyes contain chromophoric groups and aromatic rings, and their stable π-conjugated azo bond and resonance properties make them highly resistant to degradation by light and harsh environments. Consequently, they find applications in chemical industries, textile dyeing, paper production, cosmetics, and pharmaceuticals [3,4].

The global production of dyes, including azo dyes, is substantial, reaching up to 108 tons annually, with azo dyes accounting for 60-70% of the total. This extensive use results in a large volume of wastewater contaminated with azo dye pollutants. Congo Red, a diazo dye, is known to contain an aromatic amine in its structure and is recognized as a carcinogen [5]. Azo dyes, with their aromatic structures, persist in the environment for a long time, posing negative effects on both fauna and flora. Therefore, the treatment of wastewater contaminated with Congo Red dyes is imperative [6,7].

Various methods have been proposed to remove congo red from polluted water, including adsorption, coagulation-flocculation, ultrasound irradiation, ion exchange, mineralization, and photocatalysis [8-13]. Among these methods, adsorption is particularly attractive due to its low cost, abundance of available adsorbents, high adsorption capacity, ease of regeneration, and minimal energy requirements. [14] The selection and characteristics of the adsorbent play a crucial role in the adsorption process. Extensive research has been conducted to explore the use of different adsorbents for the removal of Congo Red dye from wastewater [15].

Several studies have investigated the removal of congo red (CR) from water using different adsorbents such as pristine lignin, malt bagasse, kaolin, magnetic activated carbon, and coconut shell carbon [16-18]. However, researchers are continuously searching for new adsorbents with excellent characteristics and low cost to enhance the adsorption efficiency. One promising group of adsorbent materials is derived from plant biomass. In Nigeria, sweet detar is an abundant resource, and its fruits, kernel oil, and leaves have been traded actively, particularly among rural communities. The wooden shell of the desert date seed is typically discarded as waste. To address this disposal issue, converting the seed shell into activated carbon is a potential solution. Activated carbon has been widely used for reclaiming wastewater contaminated with pollutants. Previously, there have been no reports on the removal of congo red using activated carbon derived from sweet detar seed shell. Therefore, the aim of this research is to investigate the removal of CR from aqueous solutions using activated carbon produced from sweet detar seed shell.

2. Materials and Methods

2.1. Preparation and characterization of activated carbon

The activated carbon was prepared following a procedure similar to the one described in reference [19], using sulphuric acid as the chemical activator. Locally sourced sweet detar seed shells were thoroughly washed, dried in an oven, and reduced to a particle size of 1 mm. The sample was then impregnated with 30% sulphuric acid solution for 24 hours and allowed to dry. The sample was then carbonized at 400^0C for 2 hours using muffle furnace. The activated carbon was then washed with distilled water until washings were neutral and oven dried at 1050C to constant weight and grinded into the powdered form of activated carbon and leveled properly in appropriate containers.

The surface structure was analyzed using a scanning electron microscope (PRO: X: Phenonm World 800-07334). The sample was scanned at an accelerating voltage of 15.00 kV and 1000 times magnification. Fourier transform infrared spectroscopy was used to identify the different function group present in the

sample which was monitored in the whole of the fundamental IR wave number range $650 - 4000$ cm^{-1} through a spectral resolution of 8 cm^{-1} and a total number of 32 scans and pH at point of zero charge (pH$_{pzc}$) used to determine the surface charge of the sample.

2.2. Preparation of adsorbate solution

Congo (CR) obtained from Sigma Aldrich England was used as the adsorbate without further purification. A stock solution of CR with a concentration of 1000 mg/L was prepared by dissolving 1.0 g of the dye in 1000cm3 of distilled water using a standard graduated flask. Working solutions of CR with different concentrations were prepared by diluting the stock solution using a successive dilution method. The initial pH of the aqueous phase was adjusted accordingly using 0.1 M NaOH or 0.1 M HCl solutions, and the pH was monitored using a pH meter (3510 model, Jenway).

2.3. Analysis of crystal violet

The concentration of CR in the supernatant obtained after adsorption was determined using a UV/Vis spectrophotometer (Labda 35; Perkin Elmer) at the maximum absorbance wavelength (λmax) of 498.01 nm. Standard solutions of CR with concentrations ranging from 2 to 12 mg/L were prepared, and their absorbance values were recorded to generate a calibration curve. The residual concentration of the dye in the solution was determined by interpolating the absorbance value on the calibration curve.
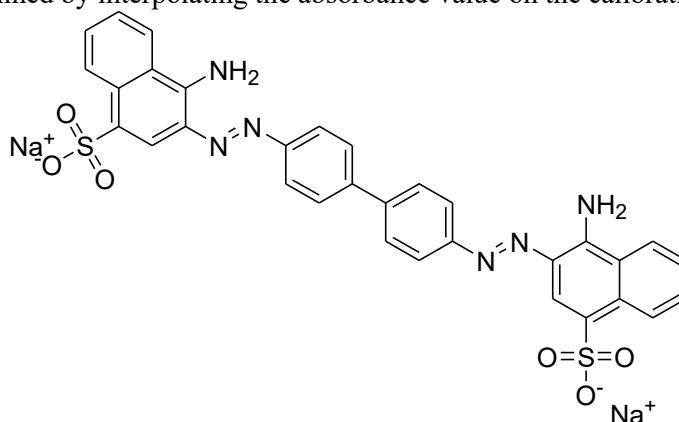

Fig. 1. Structure of Congo red

2.4. Experimental procedure

Batch adsorption experiments were performed using an Innova 4000 shaker (New Brunswick Scientific). The range of CR dye removal was studied to investigate the removal and analyze the effects of various operational parameters, including temperature (303-323 K), contact time (5-150 min), and initial adsorbate concentration (10-500 mg/L). Each parameter was individually varied while keeping the other factors constant to assess their influence on the adsorption process. In each experiment, 50 mL of adsorbate solution with a fixed concentration was mixed with 0.1 g of SDAC in a 250 mL conical flask. The pH of the solution was adjusted to desirable value. The flask contents were agitated at 200 rpm under controlled particular

temperature in an incubator shaker. After specific time intervals, samples were collected and centrifuged at 5000 rpm for 10 minutes. The clear supernatant was decanted and analyzed to determine the final dye concentration. To ensure accuracy and reproducibility, all experiments were performed in triplicate under identical conditions. The extent of dye adsorption at equilibrium, qe (mg/g), waere calculated using equation 1;

$$qe = \frac{(C_0 - C_e) \times v}{m} \qquad (1)$$

Where Co and Ce (mg/L) represent the initial and equilibrium concentrations of the liquid phase, respectively. V is the volume of the dye solution (L), and m is the dry mass of the adsorbent (g).

2.4.1. Adsorption Isotherm Studies

The obtained isotherm data for CR adsorption on SDAC were fitted to various isotherm models, including Freundlich, Langmuir, Elovich, Dubinin-Radushkevic, Jovanovic, and Temkin models. The linear form representing these models are presented as Equations 2-9. [20]

Freundlich
$$\ln q_e = \ln K_f + \frac{1}{n} \ln C_e \qquad (2)$$

Langmuir
$$\frac{1}{q_e} = \frac{1}{q_{max} K_L C_e} + \frac{1}{q_{max}} \qquad (3)$$

$$R_L = \frac{1}{1 + K_L C_0} \qquad (4)$$

Elovich
$$\ln \frac{q_e}{C_e} = \ln K_e \, q_m - \frac{q_e}{q_m} \qquad (5)$$

Dubinin- Radushkevich (D-R)
$$\ln q_e = \ln q_m - \beta \, \varepsilon^2 \qquad (6)$$

$$\varepsilon = RT\ln \left[1 + \frac{1}{C_e} \right] \text{ and } E = \frac{1}{\sqrt{2\beta}} \qquad (7)$$

Jovanovic
$$\ln q_e = \ln q_m - K_j \, C_e \qquad (8)$$

Temkin
$$q_e = B_T \ln C_e + B_T \ln K_T \qquad (9)$$

Harkin-Jura
$$\frac{1}{q_e^2} = \frac{B}{A} - \frac{1}{A} \log C_e \qquad (10)$$

In the equations, K_F, K_L, K_e, K_J, and K_T represent the isotherm constants for the Freundlich, Langmuir, Elovich, Jovanovic, and Temkin models, respectively. q_e and q_m represent the equilibrium and maximum monolayer adsorption capacities (mg/g) of SDAC, while C_e (mg/L) represents the equilibrium CR concentration. The parameters ε, β (mol²/J²), and b (J/mol) are associated with the adsorption energy. B and A are Harkin-Jura constants obtained. The suitability of each isotherm equation is evaluated by comparing the coefficients of determination, R^2.

2.4.2. Kinetic analysis

The kinetics of CR removal were evaluated using the pseudo-first-order, pseudo-second-order, Elovich Equation and Intra-particle Diffusion Equation models. The linear forms of these models are represented by Equations 11-12;

$$\ln (q_e - q_t) = \ln q_e - k_1 t \tag{11}$$
$$\frac{t}{q_t} = \frac{1}{k_2 q_e^2} + \frac{t}{q_e} \tag{12}$$

Where, k_1 (1/min) and k_2 (g/mg min) are the rate constants for the pseudo-first-order and pseudo-second-order models, respectively. The value of k_1 can be determined from the slope of the graph of $\ln(q_e - q_t)$ against t, while k_2 and q_e can be obtained from the intercept and slope of the linear plot of t/qt against t, respectively.

$$q_t = k_{id}\, t^{\frac{1}{2}} + C \tag{13}$$

Where, the constant K_{int} (mg.g^{-1} min$^{-1/2}$) represents the rate of intra particle diffusion, and C represents the thickness of the boundary layer. If the rate-limiting step is solely governed by intra particle diffusion, the plot of q_t against $t^{\frac{1}{2}}$ will exhibit a linear relationship passing through the origin.

$$q_t = \frac{\ln (\alpha \times \beta)}{\beta} + \frac{\ln (t)}{\beta} \tag{14}$$

The parameters alpha (α) and beta (β) can be determined by analyzing the slope and intercept of the linear relationship between qt and ln(t).

The goodness of fit and applicability of each kinetic model were assessed using the coefficient of determination (R^2).

2.4.3 Thermodynamic Studies

The thermodynamic parameters, including Gibbs free energy change (ΔG), entropy change (ΔS) and enthalpy change (ΔH) were calculated using Equations 15-17;

$$\Delta G = \Delta H - T\Delta S \tag{15}$$
$$K_c = \frac{C_{ads}}{C_e} \tag{16}$$
$$\ln K_c = \frac{\Delta S}{R} - \frac{\Delta H}{RT} \tag{17}$$

In these equations, C_{ads} and C_e (mg/L) represent the equilibrium of CR concentration on the SDAC and in the liquid phase respectively. K_C represents the equilibrium constant of adsorption. R represents the gas constant (8.314 J/(K·mol), and T represents the temperature (K). The values of ΔS and ΔH were determined from the slope and intercept of the plot of ln K_C against 1/T [20, 21].

3. Result and Discussion

3.1. Adsorbent Characterization

3.1.1. SEM Analysis

SEM analysis of the sample was performed to observe any morphological and surface characteristics resulting from the conversion of the precursor into activated carbon. In Fig. 2(a), the surface of sweet detar seed shell (SDSS) precursor material appeared rough and non-porous with some crevices. However, Fig. 2(b) showed that the surface texture of the precursor changed after the activation process, with prominent pores present on the surface of the activated carbon (SDAC). These pores were formed due to the

decomposition of certain lignocellulosic components at high activation temperatures and the subsequent removal of thermally labile compounds [22]. The loaded adsorbent was also analyzed, and notable changes were observed, as depicted in Fig. 2(c), it can be observed that the number of pores decreased, which could be attributed to the adsorption of dye molecules occupying the surface of the adsorbent.
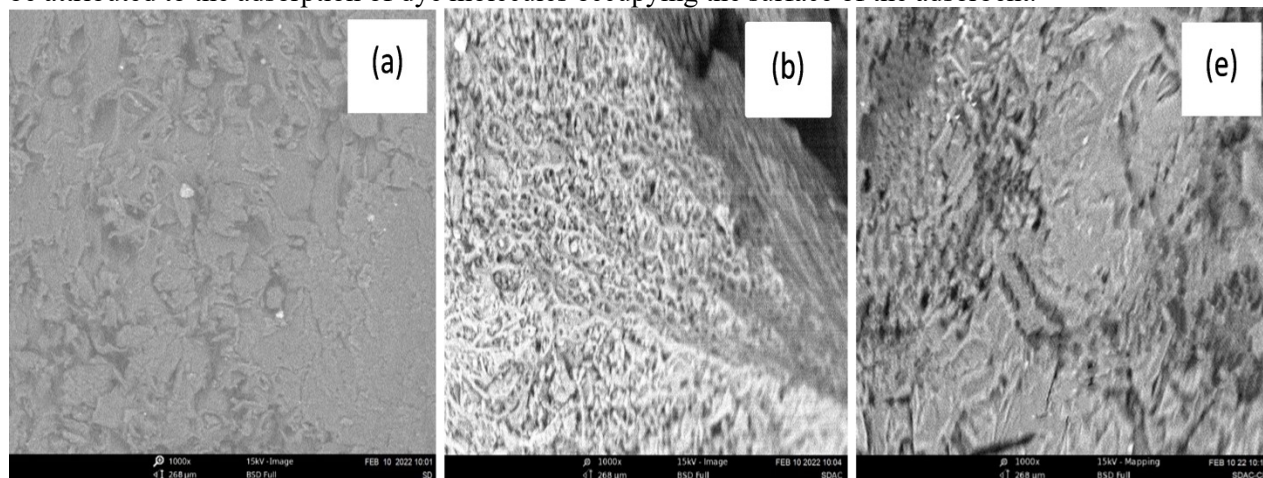

Fig. 2. SEM micrograph of (a) SDSS (b) SDAC (c) SDAC - CR.

3.1.2. FT-IR Analysis

To investigate the presence of potential adsorption sites, FTIR analysis was conducted. The FTIR spectra of SDAC before and after the adsorption of CR were examined (Fig. 3) and observed shifts in wave numbers are presented in Table 1. The appeared vibrational bands confirmed the presence of functional groups associated with cellulose, hemicellulose, pectin, and lignin, which are the main constituents of the adsorbents [23]. After adsorption, there were noticeable shifts and broadening of absorption peaks, indicating the involvement of the functional groups in the adsorption process. The shifts and changes in wavelength between the pre- and post-adsorption spectra indicate the participation of these groups in the adsorption process. Therefore, it can be concluded that the structure of the adsorbent remained unchanged during adsorption, while the dye was adsorbed onto the adsorbent surface without significant alterations to their chemical structures. This suggests that the adsorption process might be attributed to electrostatic interactions and other weak interactions between the functional groups on the adsorbent surface and adsorbate molecules.
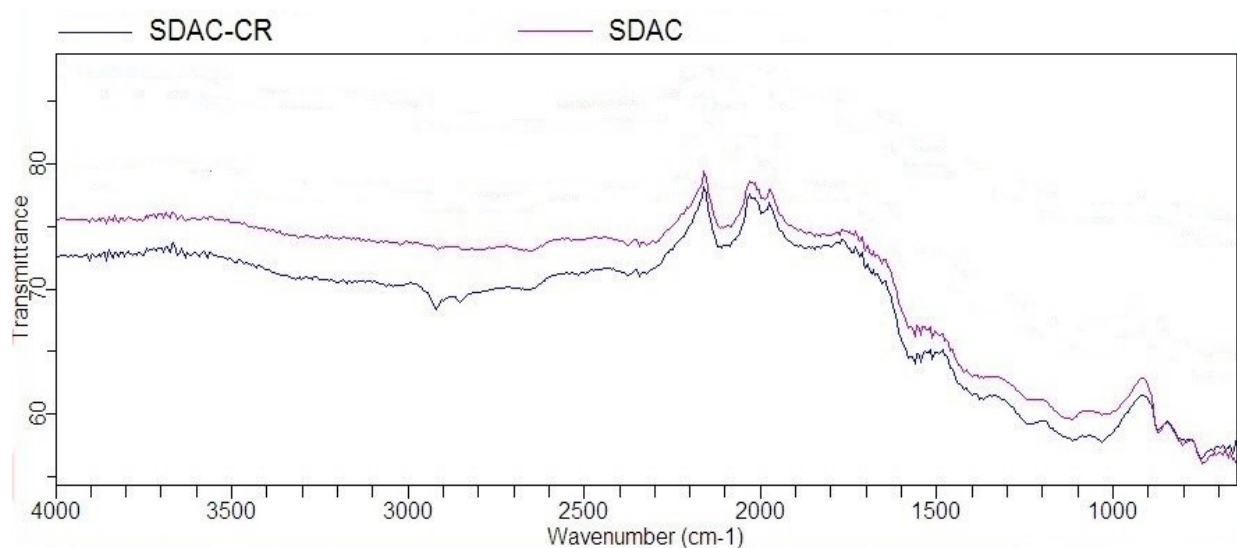
Fig. 3. FTIR Spectra of SDAC and SDAC – CR

Functional group	Wavelength range (cm^{-1})	Before Adsorption	After adsorption
O-H stretching vibration in alcohol	3700-3584	3651	3633
C-H stretching vibration in alkane	3000-2840	2910	2960
$C \equiv C$ stretching vibration in alkyne	2260-2100	2248	2220
$C \equiv C$ stretching vibration in alkyne	2260-2190	2117	2178
$C = O$ stretching of carboxylic acid	1720-1706	1704	1998
$C = O$ stretching of ketone	1685-1666	1685	1741
N-O stretching of nitro groups	1550-1500	1550	1548
C-O stretching of alcoholic groups	1124-1087	1110	1165
C-H bending of 1,3-disubstituted	880±20	873	877
C-H bending of monosubstituted	750±20	747	3633

3.1.3. Point of Zero Charge (pH$_{pzc}$)

The point of zero charge (pH$_{pzc}$) plays a significant role in determining the pH range in which an adsorbent exhibits sensitivity and indicates the type of active surface centers and their adsorption capacity. Numerous researchers have investigated the pH$_{pzc}$ of adsorbents derived from agricultural solid wastes to gain a better understanding of the adsorption mechanism. In the case of cationic dye adsorption, a pH greater than pH$_{pzc}$ is favorable due to the presence of functional groups like OH− and COO− groups. On the other hand, for anionic dye adsorption, a pH lower than pH$_{pzc}$ is preferred as the surface becomes positively charged [24]. Fig. 4, illustrates that the point of zero charge for SDAC was determined to be 5.9 Below this pH, the surface of the adsorbent acquires a positive charge, which enhances the adsorption of negatively charged dye (CR). This finding aligns with the results obtained by previous researches [25].
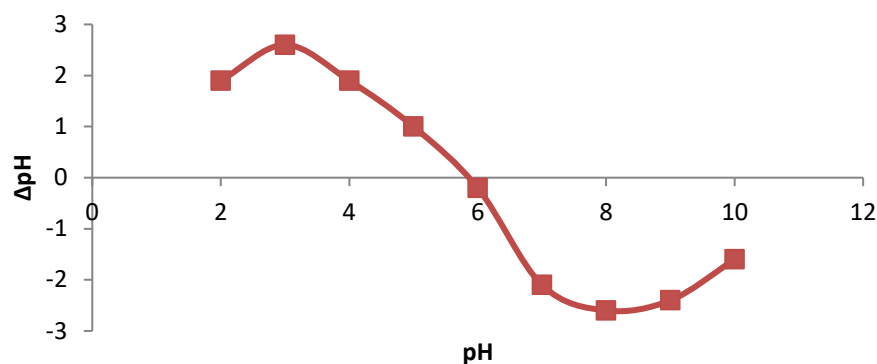
Fig.4. pH at Point of Zero Charge of SDAC

3.2. Isotherm Studies

Studies on isotherms provide valuable insights into the distribution of solute molecules between the aqueous and solid phases when they reach equilibrium. Figures 5(a-f) commonly depict the isotherms for dye adsorption at a temperature of 303 K, and Table 2 provides the values of the empirical constants that characterize the isotherms. Analysis of the correlation coefficients suggests that the Freundlich model best fits the isotherm data for CR adsorption onto SDAC. The preferred order of fitting is as follows: Freundlich > Langmuir > Jovanovic > Temkin > D-R > Elovich > Harjin - Jura. The applicability of the Freundlich isotherm indicates that the adsorbate forms multiple layers on the heterogeneous surface of the adsorbent. Additionally, the 1/n value of 0.51 indicates higher heterogeneity and suggests that physical adsorption dominates the uptake of the dye by the porous carbon [26]. The Langmuir model also provides a relatively good fit ($R^2 = 0.9555$), indicating partial involvement of a monolayer adsorption mechanism in the process. The obtained R_L value of 0.21 indicates favorable adsorption of CR onto activated carbon [27]. The equilibrium data also fits well with the Jovanovic model ($R^2 = 0.8977$) suggesting multilayer adsorption. The equilibrium data partially fits with the Elovich model ($R^2 = 0.8252$) suggesting multilayer adsorption. The poor fit of the data to the Harkin-Jura model suggests that the model is not suitable for interpreting the results. The Temkin isotherm was used to determine the energy associated with the CR-SDAC interaction, and the obtained Temkin constant value, b (0.75 kJ/mol), indicates the physical nature of the adsorption, consistent with the multilayer principle [28]. The adsorption energy E from the D-R model (0.71 kJ/mol) is less than 8 kJ/mol, indicating that weak physical forces govern the adsorption process [29].
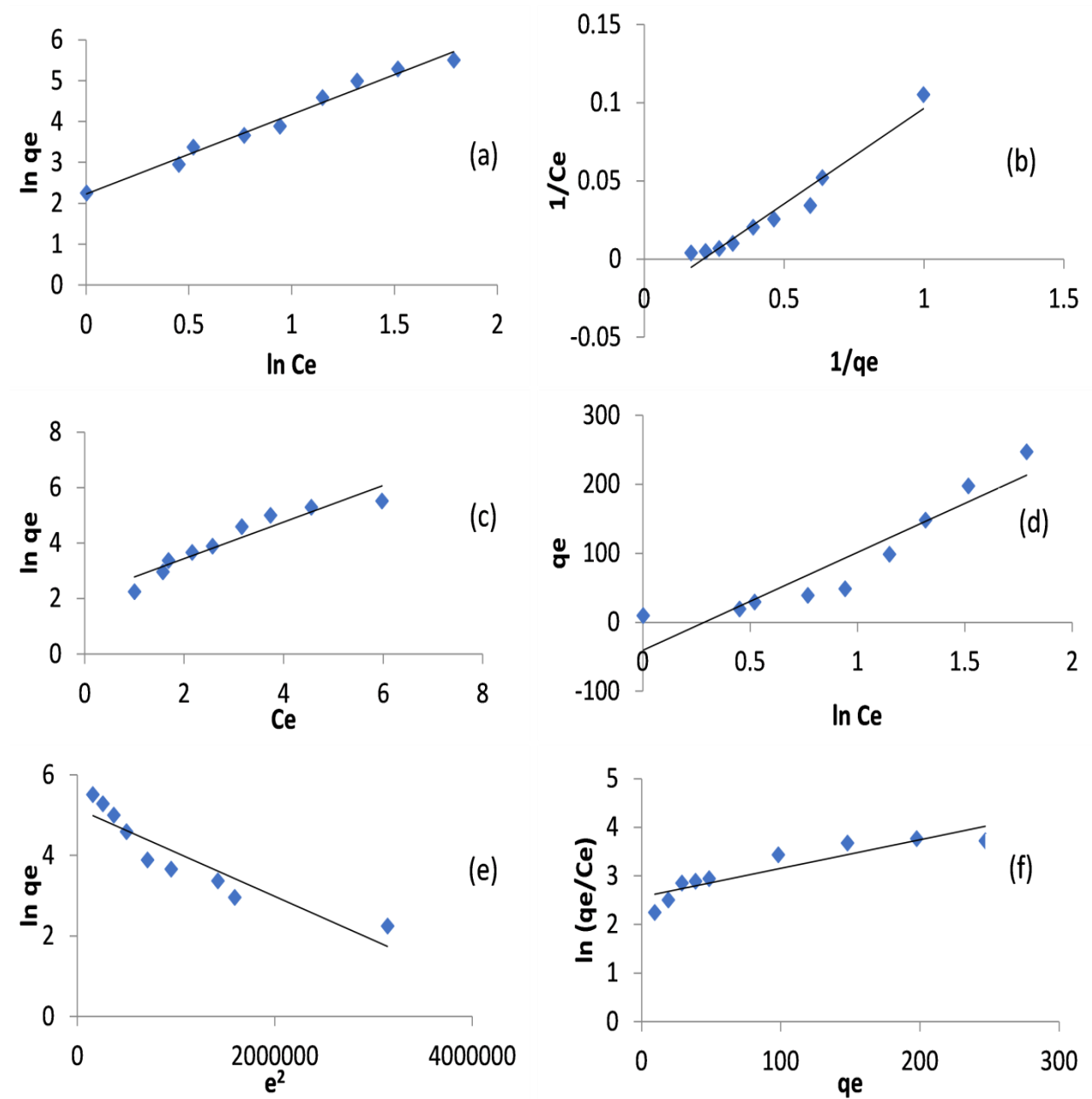
Fig.5. Isotherm fits for (a) Freundlich (b) Langmuir (c) Jovanovic (d) Temkin (e) Dubinin-Radushkevich and (f) Elovich isotherm models.

Table 2: Adsorption Isotherm Parameters

Isotherm Model	Parameters	Values
Langmuir	q_m (mg/g)	38.91
	K_L (L/mg)	0.21
	R_L	0.19
	R^2	0.9555
Freundlich	K_F (mg/g)(L/mg)$^{1/n}$	9.25
	n	1.96
	1/n	0.51
	R^2	0.9915
Temkin	K_T (L/mg)	0.75
	b_T (kJ/mol)	141.75
	R^2	0.8708
D-R	q_m (mg/g)	173.52
	β (mol^2/J^2	1×10^{-6}
	E (kJ/mol)	0.71
	R^2	0.8487
Harkin Jura	B	0.57
	A	90.91
	R^2	0.5698
Jovanovic	q_m (mg/g)	5.15
	K_J	0.66
	R^2	0.8979
Elovich	q_m (mg/g)	169.49
	K_E (L/mg)	1.01
	R^2	0.8252

3.3. Kinetic Analysis

Analysis of the kinetics of the system was carried out, and the results are presented in Fig. 6(a-d) along with the corresponding data in Table 3.

3.3.1. Pseudo-first order kinetic model

This model is suitable for liquid/solid systems and assumes that the rate of adsorption is proportional to the number of unoccupied sites on the adsorbent. The correlation coefficient (R^2) indicated that the pseudo-first order kinetic model did not adequately describe the adsorption process. Additionally, the calculated theoretical $q_{e,cal}$ value from this model does not aligns well with the experimental value.

3.3.2. Pseudo-second order kinetic model

This model assumes rate of adsorption depends on the amount of adsorbate on the surface of the adsorbent and the equilibrium adsorbed amount. It is evident that the experimental data closely match the pseudo-second-order model, with a high correlation coefficient (R^2 = 0.9995) for all. Additionally, the calculated theoretical $q_{e,cal}$ value from the pseudo-second-order model aligns well with the experimental value, indicating that the model accurately describes the observed kinetics.

3.3.3. Elovich kinetic model

This model describes chemisorption, where the rate of adsorption decreases exponentially as the amount of adsorbate increases. It provides information about surface activity and activation energy. The Elovich kinetic parameters α and β are parameters are presented in Table 2 and low correlation coefficient (R^2 = 0.9513) indicate that this model is not fit to interpret the experimental result.

3.3.4. Intraparticle diffusion equation

The Adsorption process typically consists of four stages: (a) the movement of the adsorbate from the solution to the liquid film surrounding the adsorbent, (b) the mass transfer of the adsorbate across the liquid film to the outer surface of the adsorbent, known as boundary layer diffusion or film diffusion, (c) the transport of the adsorbate from the outer surface into the pores of the adsorbent, referred to as pore diffusion or intra-particle diffusion, and (d) the adsorption of the adsorbate onto active sites on the interior and exterior surfaces of the adsorbent.

To determine the rate-controlling step in the CR removal process, the intra-particle diffusion was utilized. This model describes mass transfer in a homogenous sphere and considers the rate-determining step in an adsorption process, often associated with pore and intra-particle diffusion. As the pseudo-first and pseudo-second order models do not provide information about intra-particle diffusion, the intra-particle diffusion model can be used.
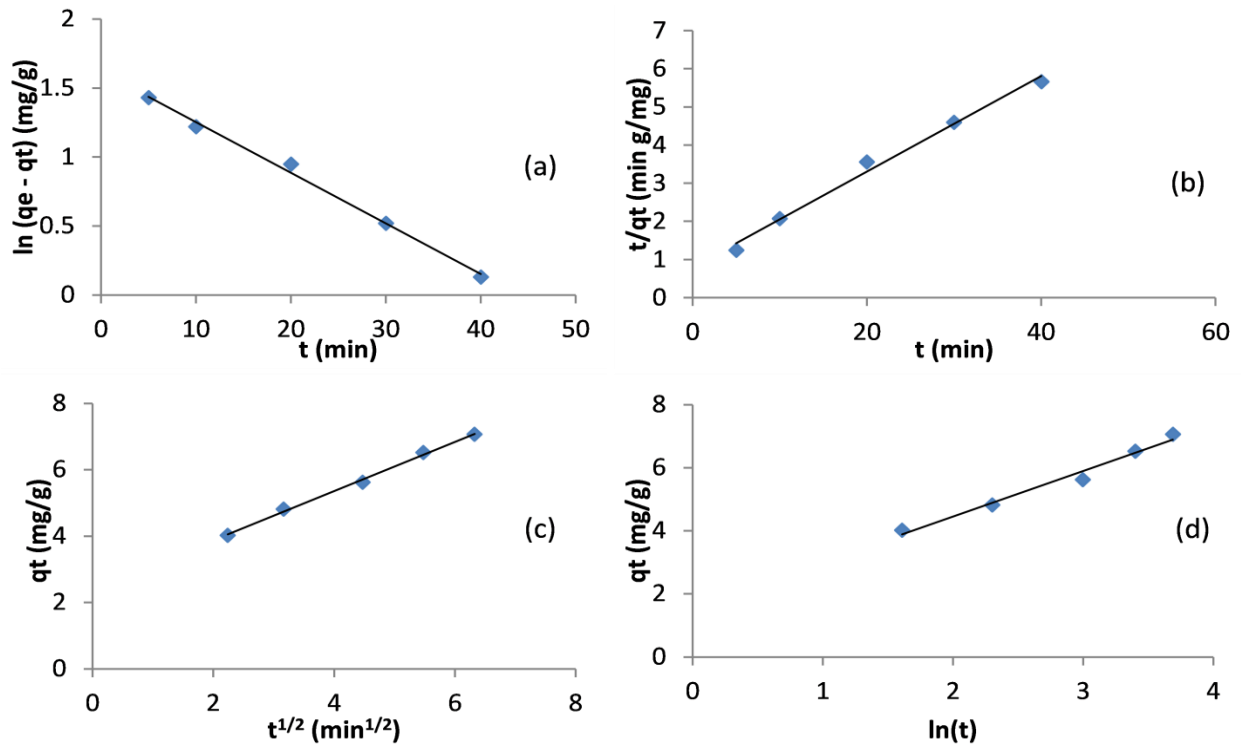
Fig.6. Pseudo-first order (a), pseudo-second order (b) Intra particle diffusion and (c) (d) Linear plots for the kinetics of CR adsorption onto CPH

Table 3: Kinetic Parameters for the Adsorption of CR

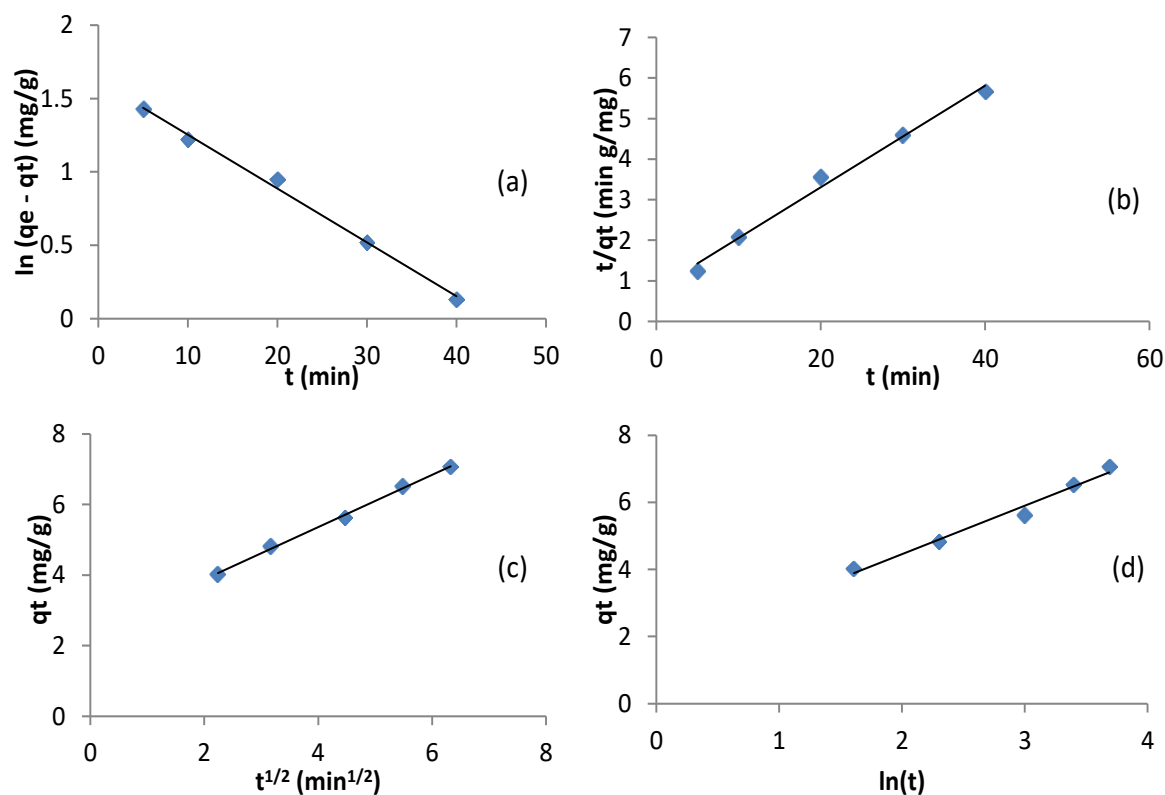| Kinetic Model	Parameters	CR
Pseudo-first order	$k_1(min^{-1})$	0.05
	$q_{e\ exp}$ (mg/g)	9.43
	$q_{e\ cal}$ (mg/g)	2.84
	R^2	0.9602
Pseudo-second order	K_2 (g/ mg min)	0.05
	$q_{e\ exp}$ (mg/g)	9.43
	$q_{e\ cal}$ (mg/g)	9.43
	R^2	0.9995
Intra-particle diffusion	k_{id} (mg/g min$^{1/2}$)	0.50
	C (mg/g)	6.03
	R^2	0.8970
Elovich	β (g/mg)	0.18
	R^2	0.9513

Fig.6. Linear plots for the kinetics of CR adsorption onto SDAC (a) Pseudo-first order (a) pseudo-second order (b) Intra particle diffusion (c) and (d) Elovich.

3.4. Thermodynamic Studies

Thermodynamic analysis provides further insights into the energy-related changes occurring during the adsorption process. The Gibbs free energy (ΔG) values were evaluated using equation 14 and other thermodynamic parameters including enthalpy change (ΔH) and ΔS were determined using the plot presented in Fig. 7. As shown in Table 4, the negative value of ΔG indicates that the removal of CR is a spontaneous process. The positive value of ΔH indicates that the adsorption of CR by the adsorbent is an endothermic process. The magnitude of the enthalpy change provides insights into the nature of the adsorption process. If ΔH exceeds 80 kJ/mol it suggests chemisorption, which involves chemical bonding between the adsorbate and the adsorbent surface. Conversely, when ΔH is below 80 kJ/mol, it indicates physisorption. In this study, the value of ΔH (-48.77 kJ/mol) suggests physisorption of the adsorbate onto SDAC. The negative value of ΔS indicates a reduction in the number of possible configuration or freedoms available to the adsorbed species.
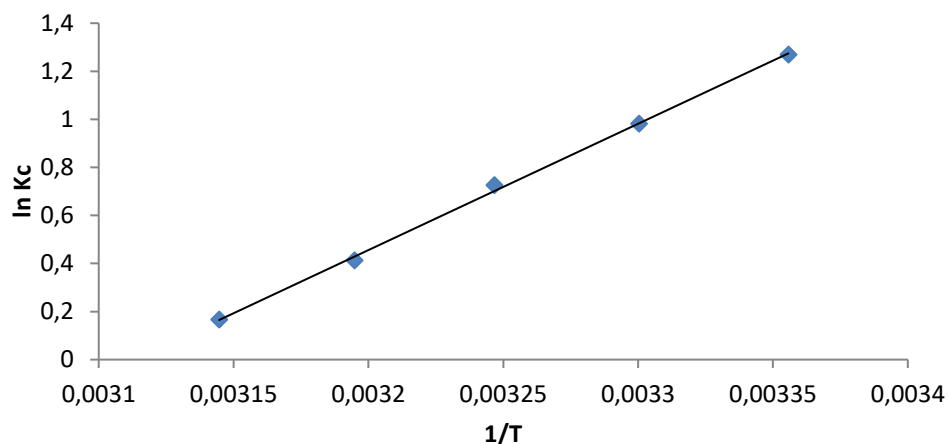
Fig. 7. Van't Hoff plot

Table 4: Thermodynamic Parameters for the Adsorbates Adsorption onto SDAC

Adsorbate	Temperature (K)	ΔG (kJ/mol)	ΔH (kJ/mol)	ΔS (kJ/K)	R^2
	303	-6.52			
	308	-5.82			
MO	313	-5.12	-48.77	-0.139	0.9953
	318	-4.42			
	323	-3.73			

4. Conclusion

The activated carbon was produced from *Detarium microcarpum* seed shell using a chemical activation method with phosphoric acid. Examination of the activated carbon and the precursor material through SEM analysis clearly illustrates the morphological differences. The FT-IR analysis showed the shifts and changes in wavelength between the pre- and post-adsorption spectra which indicated the participation of these groups in the adsorption process. The kinetics of the congo red (CR) adsorption process closely adhered to the pseudo-second-order model from the high correlation coefficient obtained. The equilibrium data were best represented by the Freundlich model indicating that CR formed multiple layers on the heterogeneous surface of SDAC. The preferred sequence of isotherm models ranked by goodness of fit was found to be Freundlich > Langmuir > Jovanovic > Temkin > Dubinin-Radushkevich (D-R) and Elovich. The values of ΔG, ΔS and ΔH from thermodynamic analysis indicated the feasibility, a reduction in the number of possible configuration or freedoms available to the adsorbed species and exothermic nature of the entire process.

Conflicts of Interest

The authors declare that they have no competing interests

References

1. Adam AM. *Curr. Comput.-Aided Drug Des.* 11(8)(*2021*)960. https:// doi. org/ 10. 3390/ cryst 11080 960.

2. Lade H, Govindwar S. & Paul D. *Int. J. Environ. Res. Public Health.* 12(6)(2015)6894–6918.

3. Mohajershojaei K, Mahmoodi NM, & Khosravi A. *Biotechnol. Bioprocess. Eng.(* 2015)109–116. https:// doi. org/ 10. 1007/ s12257- 014- 0196-0.

4. Mahmoodi, NM, Taghizadeh A, Taghizadeh M, Abdi J. *J. Hazard. Mater.* 378(2019)120741. https:// doi. org/ 10. 1016/j. jhazm at. 2019. 06. 018.

5. Mahmoodi NM, *Water Air Soil Pollut.* 224(7)(*2013*)1–8. https:// doi. org/ 10. 1007/ s11270- 013- 1612-3.

6. Hosseini SA, Vossoughi M, Mahmoodi NM, Sadrzadeh M. *J. Clean. Prod.* 183(*2018*)1197–1206. https:// doi. org/ 10. 1016/j. jclep ro.

7. Mahmoodi NM, Mokhtari-Shourijeh Z, *Fibers Polym.* 16(9)(2015)1861–1869. https:// doi. org/ 10. 1007/ s12221- 015- 5371-1

8. Mahmoodi NM, Hayati B, Arami M. *J. Chem. Eng. Data* 55(11)(*2010*)4638–4649. https:// doi. org/ 10. 1021/ je100 2384.

9. Hayati, B, Mahmoodi NM. *Desalin. Water Treat.* 47(1–3)(*2012*)322–333. https:// doi. org/ 10. 1080/ 19443 994. 2012. 696429.

10. Nodehi R, Shayesteh H, Kelishami AR. *Microchem. J.* 153(*2019*)104281. https:// doi. org/ 10. 1016/j. microc.

10. Lafi R, Montasser I, Hafiane A. *Adsorpt. Sci. Technol.* 37(*2019*)160–181.

11. Litefti K, Freire MS, Stitou M. Gonzalez-Alvarez J. *Sci. Rep.* 9(*2019*)16530. https:// doi. org/ 10. 1038/ s41598- 019- 53046-z.

12. Chatterjee S. *Sci. Rep.* 10(*2020*)111. https:// doi. org/ 10. 1038/ s41598- 019- 57017-2.

13.Li Z. *et al. Chem. Eng. J.* 388(*2020*)124263. https:// doi. org/ 10. 1016/j. cej. 2020. 124263.

14. Yang, K. *et al. Mater. Res. Express* 7(*2020*)015103. https:// doi. org/ 10. 1088/ 2053- 1591/ ab5ff3

15. Jia, Y. *et al. J. Chem. Eng. Data* 65(2)(*2020*)725–736. https:// doi. org/ 10. 1021/ acs. jced. 9b009 51.

16. Reis HC, Cossolin AS, Santos BA, Castro KC, Pereira GM, Silva VC, Sousa PT, Dall'Oglio Vasconcelos EL, Morais LG, Malt EB. *International Journal of Biotechnology and Bioengineering.* 12(4)2018)118-126.

17. Caponi N, Collazzo GC, Jahn SL, Dotto GL, Mazutti MA, Foletto EL. *Materials Research.* 20(2017)14-22.

18. Rinku J, Shripal S, Hemant P. R*esearch Journal of Chemical Sciences*. 5(12)(2015)38-43.

19. Jadhav SK, Thorat SR. *Biosciences biotechnology research.* 19(1)(2022)141-151.

20. Husaini M, Ibrahim MB. *International Journal of Engineering and Manufacturing.* 9(6)(2019)53-64

21. Husaini M, Usman B, Ibrahim MA, Ibrahim MB. *Res. J. Chem. Environ.*, 24(2)(2020)99-106.

22. Ahmad MA, Ahmad N, Bello OS. *Water Air Soil Pollution*. 225(2014)1-18.

23. Asbollah MA, Kusrini AE. Usman A. *International Journal of Phytoremediation*. (2021)7-14. DOI: 10.1080/15226514.2021.1901851.

24. Ibrahim MB, Ahmed, A. *Bayero Journal of Pure and Applied Sciences. Special Conference Edition November. 10(1) (2017)606 - 614*

25. Ramilarasan RT, Vijayakumar G, Dharmendira KM. *J. Master.Environ.(2012)*2028-2508.

26. Pakade VE, Nchoe OB, Hlungwane L, Tavengwa NT. *Water Science and Technology*. 75(1)(2017)196-206.

27. Husaini M, Usman B, Ibrahim MB. *Journal of Science and Technology*. 11(2)(2019)8-16.

28. Kyziol-Komosinska J, Rosik-Dulewska C, Franus M, Antoszczyszyn-Szpicka P, Czupiol J, Krzyzewska I. 24 (2015)1111–23.

29. Foo KY, Hameed BH. Insights into the modeling of adsorption isotherm systems. Chemical Engineering Journal. 156(2010) 2-1.